LETTER

doi:10.1038/nature13123

Reconciliation of the carbon budget in the ocean's twilight zone

Sarah L. C. Giering[1,2,3], Richard Sanders[1], Richard S. Lampitt[1], Thomas R. Anderson[1], Christian Tamburini[4], Mehdi Boutrif[4], Mikhail V. Zubkov[1], Chris M. Marsay[2,5], Stephanie A. Henson[1], Kevin Saw[1], Kathryn Cook[6] & Daniel J. Mayor[3]

Photosynthesis in the surface ocean produces approximately 100 gigatonnes of organic carbon per year, of which 5 to 15 per cent is exported to the deep ocean[1,2]. The rate at which the sinking carbon is converted into carbon dioxide by heterotrophic organisms at depth is important in controlling oceanic carbon storage[3]. It remains uncertain, however, to what extent surface ocean carbon supply meets the demand of water-column biota; the discrepancy between known carbon sources and sinks is as much as two orders of magnitude[4–8]. Here we present field measurements, respiration rate estimates and a steady-state model that allow us to balance carbon sources and sinks to within observational uncertainties at the Porcupine Abyssal Plain site in the eastern North Atlantic Ocean. We find that prokaryotes are responsible for 70 to 92 per cent of the estimated remineralization in the twilight zone (depths of 50 to 1,000 metres) despite the fact that much of the organic carbon is exported in the form of large, fast-sinking particles accessible to larger zooplankton. We suggest that this occurs because zooplankton fragment and ingest half of the fast-sinking particles, of which more than 30 per cent may be released as suspended and slowly sinking matter, stimulating the deep-ocean microbial loop. The synergy between microbes and zooplankton in the twilight zone is important to our understanding of the processes controlling the oceanic carbon sink.

The global carbon cycle is affected by biological processes in the oceans, which export carbon from surface waters in the form of organic matter and store it at depth, in a process called the 'biological carbon pump'. Most of the exported organic carbon is processed by the water-column biota, which ultimately convert it into CO_2 by means of respiration (remineralization). Variations in the resulting decrease in organic flux with depth[9] can, according to models, lead to changes in atmospheric CO_2 of up to 200 p.p.m. (ref. 3), indicating a strong coupling between biological activity in the ocean interior and oceanic storage of CO_2.

A key constraint in the analysis of carbon fluxes in the twilight zone is that, in the steady state, the attenuation of particulate organic carbon (POC) flux with depth should be balanced by community metabolism. Published estimates of POC flux attenuation with depth are, however, up to two orders of magnitude lower than corresponding estimates of heterotrophic metabolism[4–7]. This discrepancy indicates either that estimates of POC flux, community metabolism, or both, are unreliable, or that additional, unaccounted for, sources of organic carbon to the twilight zone exist[8].

We compiled a comprehensive carbon budget of the twilight zone on the basis of an extensive programme of field measurements at the Porcupine Abyssal Plain (PAP) site (Extended Data Fig. 1a) in July and August 2009. This site is located in the transition region between the subtropical and subpolar gyres of the North Atlantic[10]. The mixed-layer depth remained constant at approximately 50 m throughout the study period. This depth was subsequently used as the upper boundary of the twilight zone, given the need to normalize export measurements to dynamic upper boundaries for the twilight zone[11].

Organic carbon sources to the twilight zone include sinking particles, downward mixing of dissolved organic carbon (DOC), lateral advection of organic matter from the continental shelf, active transport via the daily vertical migration of zooplankton that feed in the mixed layer at night and rest at depth during the day, and chemolithoautotrophy (prokaryotic growth using dissolved inorganic carbon and chemical energy sources).

The downward flux of sinking particles was measured using simultaneous 48-h deployments of free-drifting, neutrally buoyant sediment traps[12] at depths of 50, 150, 300, 450 and 600 m (Extended Data Table 1). Satellite chlorophyll imagery and horizontal velocities (obtained using a 150-kHz vessel-mounted acoustic Doppler current profiler) confirmed that all of the traps were advected along the edge of an anticyclonic eddy for 50 km before surfacing within 3.5 km of each other. The measured POC flux at 50 m (84 ± 8 mg C m^{-2} d^{-1}) was close to estimates independently derived using ^{234}Th budgets and studies of collected marine snow particles[13] (99 ± 41 and 146 ± 26 mg C m^{-2} d^{-1}, respectively). Attenuation of POC flux (F) with depth (z) was fitted to the Martin curve[9] ($F_z = F_{MLD}(z/MLD)^b$), where F_{MLD} is the flux at the bottom of the mixed layer, MLD is the depth of the bottom of the mixed layer and b is the rate of attenuation. The observed attenuation rate ($b = -0.70$; $P < 0.01$, $R^2 = 0.95$, $n = 5$) was consistent with observations in the Pacific Ocean[9,14] ($b = -0.50$ to -1.38; Fig. 1a). Downward POC flux was extrapolated to 1,000 m using $b = -0.70$. The total loss of POC within the twilight zone was 74 ± 9 mg C m^{-2} d^{-1}.

DOC input to the twilight zone was estimated to be 15 mg DOC m^{-2} d^{-1} (range, 0.4–30 mg DOC m^{-2} d^{-1}) on the basis both of the ratio between DOC concentrations and apparent oxygen utilization[15], and of DOC gradients coupled to turbulent diffusivity measured from previous work at the study site[16] (Methods and Extended Data Fig. 2). DOC was estimated to supply 17% of total export, in agreement with previous estimates of 9–20% across the North Atlantic basin[17]. Organic matter input through lateral advection was assumed to be negligible from analyses of back-trajectories (derived from satellite-derived near-surface velocities over 3 months) of the water masses arriving at the PAP site during the study period, which suggested that the water had not passed over the continental slope (Extended Data Fig. 1b). The final source of DOC, namely excretion at depth by active flux, was estimated using net samples of zooplankton biomass and allometric equations[6,18], giving a supply of 3 mg C m^{-2} d^{-1}. Defecation and mortality at depth present further sources of organic carbon to the twilight zone, but these were excluded from the budget owing to large uncertainties associated with their estimation. Finally, chemolithoautotrophy has been suggested to be an important source of organic matter in the deep ocean[19], but without strong evidence that this poorly understood process could provide a major contribution at our study site, we chose to exclude it from our carbon budget.

The remineralization of organic carbon by zooplankton and prokaryotes was estimated from zooplankton biomass and prokaryotic activity.

[1]National Oceanography Centre, University of Southampton, Waterfront Campus, European Way, Southampton SO14 3ZH, UK. [2]Ocean and Earth Sciences, University of Southampton, European Way, Southampton SO14 3ZH, UK. [3]Institute of Biological and Environmental Sciences, Oceanlab, University of Aberdeen, Newburgh AB41 6AA, UK. [4]Aix-Marseille Université, Université de Toulon, CNRS/INSU, IRD, MIO, UM 110, 13288 Marseille Cedex 09, France. [5]Department of Earth and Ocean Sciences, University of South Carolina, Columbia, South Carolina 29208, USA. [6]Marine Laboratory, Marine Scotland Science, Scottish Government, PO Box 101, 375 Victoria Road, Aberdeen AB11 9DB, UK.

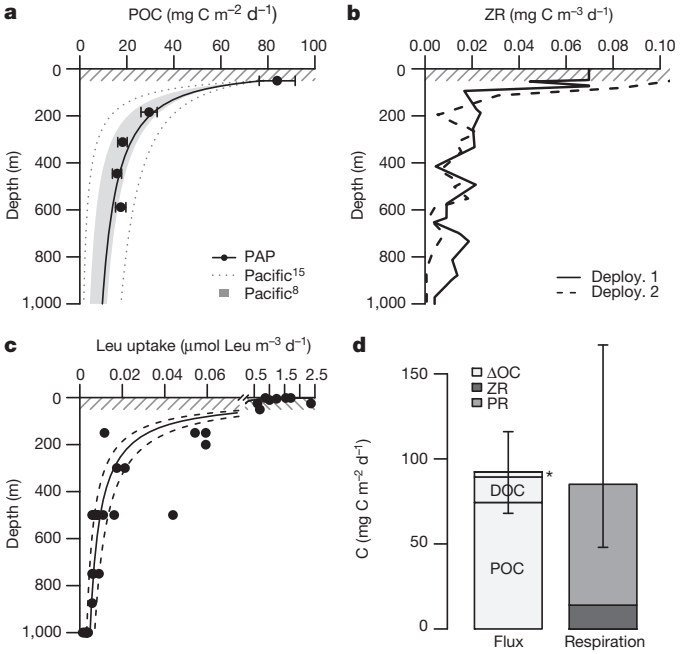

Figure 1 | Sinks and sources of organic carbon to the twilight zone. **a**, POC flux (black dots) below the mixed layer (shaded area) at the PAP site during 3–6 August 2009, fitted to the Martin equation ($F_z = F_{50}(z/50)^b$; solid line; $F_{50} = 78$ mg C m^{-2} d^{-1}, $b = -0.70$; $P < 0.01$, $R^2 = 0.95$, $n = 5$). The observed attenuation is consistent with rates observed in the Pacific[9,14] (grey area, dotted lines). Error bars show analytical error (s.d.). **b**, **c**, Depth profiles of respiration by non-migratory zooplankton (ZR) based on biomass samples ($n = 58$; **b**) and leucine incorporation (μmol Leu m^{-3} d^{-1}) by prokaryotes (power-law fit (solid) and interquartile range (dashed); $P < 0.001$, $R^2 = 0.86$, $n = 37$; **c**). **d**, The sum of net organic carbon supply (ΔOC; light grey) of POC, DOC and active flux (asterisk) matches respiration by non-migratory zooplankton (ZR; dark grey) and prokaryotes (PR; mid grey). Error bars represent upper and lower estimates (see text and Table 1).

It is crucial to note that in a steady-state system, such as we assume this to be, organic carbon is lost from the system only by export or by remineralization. We focus entirely on community respiration as a measure of remineralization, which is a fundamental advance over previous methods to derive budgets (Methods).

Zooplankton respiration was estimated by applying allometric relationships[6] to biomass measurements derived from net samples collected vertically every 80 m, twice during both day and night, using the ARIES net system fitted with 200-μm cod-ends (the narrow, exchangeable ends of the nets, which retain the samples) (Extended Data Table 1 and Extended Data Fig. 3). These allometric relationships are well constrained[6], but they are based on epipelagic zooplankton and our calculated respiration rates for the lower mesopelagic are therefore probably overestimates of the true rates[20]. Zooplankton resident in the twilight zone, mostly detritivorous copepods (*Oithona* and *Oncaea*) and carnivorous chaetognaths, had combined respiration rates of 15.2 and 12.7 mg C m^{-2} d^{-1} (50–1,000 m), respectively, during the two deployment periods (Fig. 1b). Migrating zooplankton (determined as the difference between day and night biomasses) were excluded from these estimates because we assume that they ingest sufficient carbon during grazing at the surface to satisfy their diagnosed respiration rates at depth (Methods). The organic carbon they respire within the twilight zone is thus imported by daily vertical migration.

Prokaryotic heterotrophic production was determined using bioassay isotope-dilution techniques with ^{3}H-leucine tracer[21]. Leucine incorporation rates were 41.7 ± 21.2 nmol Leu m^{-3} d^{-1} at 150 m and 6.6 ± 4.1 nmol Leu m^{-3} d^{-1} at 500–750 m (Fig. 1c), similar to previous estimates in the eastern North Atlantic[19] (37.7 and 7.5 nmol Leu m^{-3} d^{-1}, respectively). Integrated leucine incorporation based on a power-law fit was 14.5 μmol Leu m^{-2} d^{-1} (interquartile range, 13.2–16.1 μmol Leu m^{-2} d^{-1}; $P < 0.001$, $R^2 = 0.86$, $n = 37$). This fit was chosen on the assumption that bacterial activity follows the supply of organic carbon[22], although we lack data from between 50 and 150 m to confirm this fit. The uncertainty in this interpolation possibly leads to a misestimate of integrated leucine incorporation. Integrated leucine incorporation was converted into respiration using leucine-to-carbon conversion factors (0.44 ± 0.27 kg C mol^{-1} Leu) and growth efficiencies (interquartile range, 0.04–0.12) specific to the twilight zone derived from thorough literature surveys (Methods and Extended Data Fig. 4). The uncertainty in this calculation was estimated by bootstrap analysis with 100,000 simulations. The final estimate for integrated (50–1,000 m) prokaryotic respiration was 71 mg C m^{-2} d^{-1} (interquartile range, 35–152 mg C m^{-2} d^{-1}).

The sum of the inputs from POC and DOC matches community respiration (68–116 versus 48–167 mg C m^{-2} d^{-1}; Fig. 1d), with prokaryotes dominating community respiration (70–92%; Table 1).

Our study successfully reconciles the various components of the carbon budget in the twilight zone of the ocean. This was possible because we considered a dynamic upper boundary for the twilight zone (the base of the mixed layer), excluded vertical migrators from the estimate of zooplankton respiration in the twilight zone, and compared respiration rather than carbon demand to net organic carbon supply. Depth-resolved estimates of supply and consumption (Extended Data Fig. 5) show an excess of supply in the upper twilight zone (50–150 m) and a deficit in the lower twilight zone (150–1,000 m). We suggest that this may be caused by a subtle vertical change in ecosystem structure with depth[23,24] or an unaccounted-for vertical transfer of organic carbon between the upper and lower twilight zones.

The suggestion that prokaryotes dominate community respiration seems counterintuitive given that organic carbon supply to the twilight zone is dominated by sinking particles that are accessible to larger (>200 μm) zooplankton. We therefore propose that one of the main roles of zooplankton in the twilight zone is to mechanically degrade particulate material[25] into slow-sinking particulate matter and dissolved organic material that is subsequently remineralized by microbes (prokaryotes and their consumers).

To explore whether this conceptual picture is consistent with our present understanding of twilight-zone ecology, and to provide a full quantitative picture of the twilight-zone carbon cycle, we used a simple steady-state model of that cycle[26]. The model traces the turnover and remineralization of sinking POC along three pathways: colonization and solubilization of detritus by attached microbes, production of free-living microbes following loss of solubilization products during particle degradation, and consumption by detritivorous zooplankton (Methods and Extended Data Fig. 6a). The model was modified to include vertical mixing of DOC and active transport as carbon inputs to the twilight zone and to represent POC in both sinking and suspended forms, the latter produced via zooplankton 'sloppy feeding'[27] (leakage during ingestion). Inputs of carbon to the twilight zone were the measured values given in Table 1.

Modelled respiration rates matched field data well, with 84% of the CO_2 being produced by microbes (prokaryotes and prokaryote consumers) and only 16% by zooplankton (detritivores and carnivores) (Fig. 2). The model further suggests that microzooplankton respiration,

Table 1 | Carbon budget for the twilight zone (50–1,000 m)

Input		Respiration		Community respiration (%)
Sinking POC	74 (65–83)	Zooplankton	14 (13–15)	16 (8–30)
Vertical mixing (DOC)	15 (0–30)			
Active transport (DOC)	3	Prokaryotes	71 (35–152)	84 (70–92)
Lateral advection	0			
Total	92 (68–116)		85 (48–167)	—

Input fluxes and respiration rates (mg C m^{-2} d^{-1}) are based on measurements at the PAP site. Numbers in brackets refer to lower and upper estimates (see text). Community respiration was estimated by combining highest and lowest estimates.

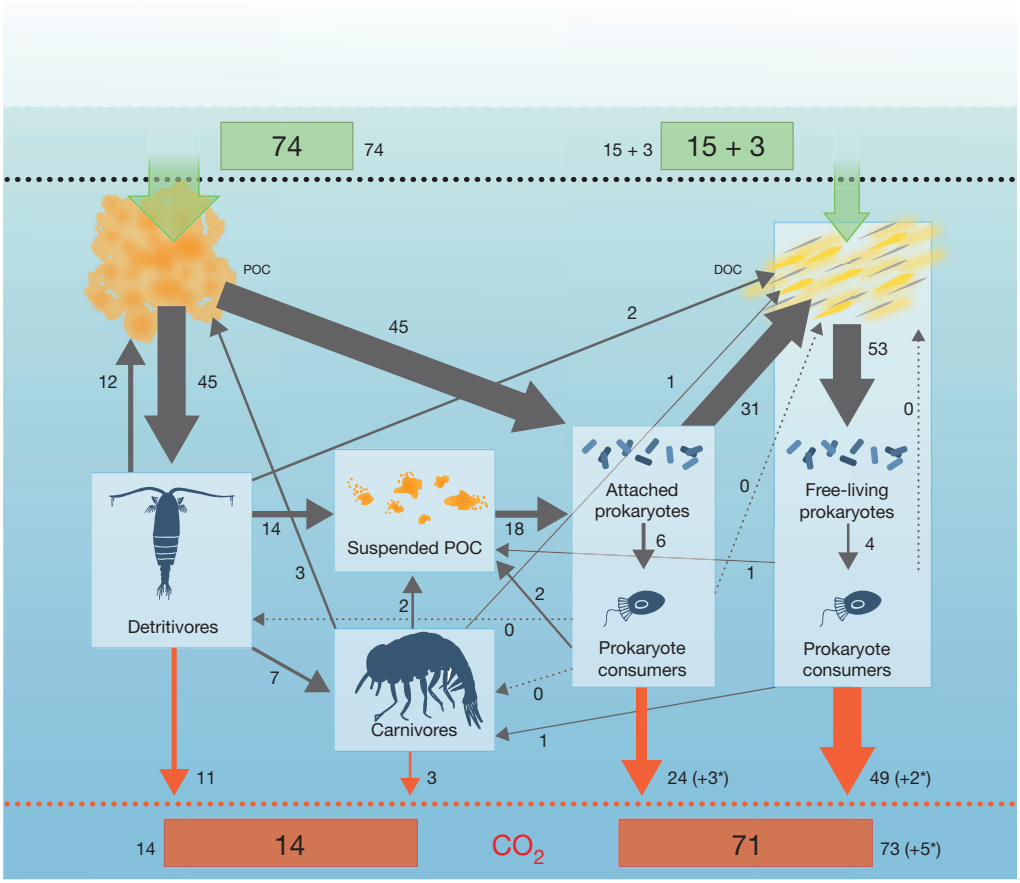

Figure 2 | Predicted carbon cycle in the twilight zone. Organic carbon is supplied to the twilight zone as POC and DOC (vertical mixing plus active transport) (green arrows). POC is processed by detritivores (50%) or attached prokaryotes (50%) and recycled in the twilight zone until eventually remineralized (red arrows), whereby prokaryotes dominate respiration (79%). Observed rates of carbon supply to the twilight zone and remineralization via respiration ('CO_2') are displayed in green and red boxes, respectively. Internal net flows (mg C m^{-2} d^{-1}) derived from a numerical model are represented as arrows (line width reflects flow magnitude; dotted lines are flows <0.5 mg C m^{-2} d^{-1}). Fluxes indicated with an asterisk are for microzooplankton (prokaryote consumers), which are not included in the measured estimates.

which had not been measured during the study, has a small role in the overall budget, contributing only 5 mg C m^{-2} d^{-1}. Attached prokaryotes processed half of the POC flux. The remaining half was processed by detritivorous zooplankton, which released 30% of it as suspended POC, thereby confirming our hypothesis. The relative roles of zooplankton and prokaryotes in processing and respiring sinking POC are robust to changing model parameter values (Methods and Extended Data Fig. 7). Moreover, it is consistent with the general perception that detritivores are sloppy feeders that ingest <40% of processed particles, causing most fast-sinking POC to break up into slow- or non-sinking POC and DOC[25]. This pool of suspended organic matter stimulates the microbial loop[28] in the twilight zone and ultimately fuels the respiration of prokaryotes[6,26].

Our results highlight a synergy between zooplankton and microbes in the twilight zone, where both are important in processing the organic carbon flux and, subsequently, in controlling the strength of the oceanic carbon sink. Large uncertainties remain, however, particularly with regard to estimating prokaryotic activity. A better understanding of prokaryotic metabolism throughout the twilight zone, combined with process studies focusing on the upper twilight zone, is necessary to understand the biological carbon pump fully.

METHODS SUMMARY

We conducted an extensive programme of field measurements at the PAP site (49.0 °N, 16.5 °W) from 8 July to 13 August 2009 aboard RRS *Discovery*. Sinking material was collected for 48 h using free-drifting, neutrally buoyant PELAGRA sediment traps[12]. Samples were screened to remove swimmers, split into aliquots, filtered onto pre-combusted glass fibre filters (grade GF/F), fumed with sulphurous acid and analysed for POC. DOC input was estimated from data collected near the PAP site during May–June 2005 (https://www.bodc.ac.uk/data/published_data_library/catalogue/10.5285/f3b3d4e9-5ede-2824-e044-000b5de50f38/) and October–November 2005 (https://www.bodc.ac.uk/data/published_data_library/catalogue/10.5285/f3b3d4e9-5edf-2824-e044-000b5de50f38/). The slope of the correlation between measured DOC and apparent oxygen utilization was compared with the theoretical slope ($C_{org}/-O_2 = 117/170$), giving the relative contribution of DOC to heterotrophic respiration[15]. A lower estimate was calculated using turbulent diffusivity measurements at the PAP site[16], coupled with the aforementioned DOC profiles. Samples for zooplankton biomass profiles (0–1,000 m at 80-m intervals) were preserved in formaldehyde, size-fractionated, identified and enumerated. One to fifty individuals from each group at each depth and size fraction were analysed for dry weight. Zooplankton respiration (in micrograms of carbon per individual per hour) was estimated as a function of body mass (in milligrams dry weight per individual) and temperature[6] (degrees Celsius). DOC excretion at depth was assumed to be equivalent to 31% of respiration by migrating zooplankton[18]. Leucine incorporation rates were estimated on samples ($n = 37$) recovered from depth using a conductivity–temperature–depth rosette sampler. Both time-course experiments and concentration-series bioassays were carried out. In these respective types of experiment, ^{3}H-leucine was added at final concentrations of 10–20 nM and 0.025–0.5 nM and incubated in the dark at *in situ* temperatures for 4–8 h and 0.5–2 h. Samples were filtered onto 0.2-μm polycarbonate filters and washed with deionized water, and their radioactivity was then measured.

The cruise metadata report is available from the British Oceanographic Data Centre (http://www.bodc.ac.uk/data/documents/cruise/9451/).

Online Content Any additional Methods, Extended Data display items and Source Data are available in the online version of the paper; references unique to these sections appear only in the online paper.

Received 8 February 2013; accepted 31 January 2014.
Published online 19 March 2014.

1. Laws, E. A., Falkowski, P. G., Smith, W. O. J., Ducklow, H. & McCarthy, J. J. Temperature effects on export production in the open ocean. *Glob. Biogeochem. Cycles* **14,** 1231–1246 (2000).
2. Henson, S. A. *et al.* A reduced estimate of the strength of the ocean's biological carbon pump. *Geophys. Res. Lett.* **38,** L04606 (2011).
3. Kwon, E. Y., Primeau, F. & Sarmiento, J. L. The impact of remineralization depth on the air–sea carbon balance. *Nature Geosci.* **2,** 630–635 (2009).
4. Boyd, P. W. *et al.* Transformations of biogenic particulates from the pelagic to the deep ocean realm. *Deep-Sea Res. II* **46,** 2761–2792 (1999).
5. Reinthaler, T., Van Aken, H. M. & Veth, C. Prokaryotic respiration and production in the meso- and bathypelagic realm of the eastern and western North Atlantic basin. *Limnol. Oceanogr.* **51,** 1262–1273 (2006).
6. Steinberg, D. K. *et al.* Bacterial vs zooplankton control of sinking particle flux in the ocean's twilight zone. *Limnol. Oceanogr.* **53,** 1327–1338 (2008).
7. Baltar, F., Aristegui, J., Gasol, J. M., Sintes, E. & Herndl, G. J. Evidence of prokaryotic metabolism on suspended particulate organic matter in the dark waters of the subtropical North Atlantic. *Limnol. Oceanogr.* **54,** 182–193 (2009).
8. Burd, A. B. *et al.* Assessing the apparent imbalance between geochemical and biochemical indicators of meso- and bathypelagic biological activity: what the @$é! is wrong with present calculations of carbon budgets? *Deep-Sea Res. II* **57,** 1557–1571 (2010).
9. Martin, J. H., Knauer, G. A., Karl, D. M. & Broenkow, W. W. VERTEX: carbon cycling in the northeast Pacific. *Deep-Sea Res. I* **34,** 267–285 (1987).
10. Henson, S. A., Dunne, J. P. & Sarmiento, J. L. Decadal variability in North Atlantic phytoplankton blooms. *J. Geophys. Res.* **114,** C04013 (2009).
11. Buesseler, K. O. *et al.* Shedding light on processes that control particle export and flux attenuation in the twilight zone of the open ocean. *Limnol. Oceanogr.* **54,** 1210–1232 (2009).
12. Lampitt, R. S. *et al.* Particle export from the euphotic zone: estimates using a novel drifting sediment trap, ^{234}Th and new production. *Deep-Sea Res. I* **55,** 1484–1502 (2008).
13. Riley, J. S. *et al.* The relative contribution of fast and slow sinking particles to ocean carbon export. *Glob. Biogeochem. Cycles* **26,** GB1026 (2012).
14. Buesseler, K. O. *et al.* Revisiting carbon flux through the ocean's twilight zone. *Science* **316,** 567–570 (2007).
15. Doval, M. D. & Hansell, D. A. Organic carbon and apparent oxygen utilization in the western South Pacific and the central Indian oceans. *Mar. Chem.* **68,** 249–264 (2000).
16. Martin, A. P. *et al.* The supply of nutrients due to vertical turbulent mixing: a study at the Porcupine Abyssal Plain study site in the northeast Atlantic. *Deep-Sea Res. II* **57,** 1293–1302 (2010).
17. Carlson, C. A. *et al.* Dissolved organic carbon export and subsequent remineralization in the mesopelagic and bathypelagic realms of the North Atlantic basin. *Deep-Sea Res. II* **57,** 1433–1445 (2010).
18. Steinberg, D. K. *et al.* Zooplankton vertical migration and the active transport of dissolved organic and inorganic carbon in the Sargasso Sea. *Deep-Sea Res. I* **47,** 137–158 (2000).
19. Reinthaler, T., Van Aken, H. M. & Herndl, G. J. Major contribution of autotrophy to microbial carbon cycling in the deep North Atlantic's interior. *Deep-Sea Res. II* **57,** 1572–1580 (2010).
20. Ikeda, T., Sano, F., Yamaguchi, A. & Matsuishi, T. Metabolism of mesopelagic and bathypelagic copepods in the western North Pacific Ocean. *Mar. Ecol. Prog. Ser.* **322,** 199–211 (2006).
21. Kirchman, D., K'nees, E. & Hodson, R. Leucine incorporation and its potential as a measure of protein synthesis by bacteria in natural aquatic systems. *Appl. Environ. Microbiol.* **49,** 599–607 (1985).
22. Ducklow, H. W., Kirchman, D. L., Quinby, H. L., Carlson, C. A. & Dam, H. G. Stocks and dynamics of bacterioplankton carbon during the spring bloom in the eastern North Atlantic Ocean. *Deep-Sea Res. II* **40,** 245–263 (1993).
23. DeLong, E. *et al.* Community genomics among stratified microbial assemblages in the ocean's interior. *Science* **311,** 496–503 (2006).
24. Iversen, M. H., Nowald, N., Ploug, H., Jackson, G. A. & Fisher, G. High resolution profiles of vertical particulate organic matter export off Cape Blanc, Mauritania: degradation processes and ballasting effects. *Deep-Sea Res. I* **57,** 771–784 (2010).
25. Lampitt, R., Noji, T. & Von Bodungen, B. What happens to zooplankton faecal pellets? Implications for material flux. *Mar. Biol.* **104,** 15–23 (1990).
26. Anderson, T. R. & Tang, K. W. Carbon cycling and POC turnover in the mesopelagic zone of the ocean: insights from a simple model. *Deep-Sea Res. II* **57,** 1581–1592 (2010).
27. Jumars, P., Penry, D. & Baross, J. Closing the microbial loop: dissolved carbon pathway to heterotrophic bacteria from incomplete ingestion, digestion and absorption in animals. *Deep-Sea Res. A* **36,** 483–495 (1989).
28. Azam, F. *et al.* The ecological role of water-column microbes in the sea. *Mar. Ecol. Prog. Ser.* **10,** 257–263 (1983).

Acknowledgements We thank the captain and crew of the RRS *Discovery* and scientists during D341, especially J. Hunter for executing the ARIES deployments and S. Ward for the PELAGRA deployments. We thank the OSCAR Project Office and BODC for providing data. Finally, we thank T. Cornulier for statistical help. This work was funded by Oceans 2025 and EU FP7-ENV-2010 Collaborative Project 264933 BASIN Basin-Scale Analysis, Synthesis and Integration. C.T. and M.B. were funded by the ANR-POTES program (no. ANR-05-BLAN-0161-01, awarded to C. T.) supported by the Agence Nationale de la Recherche (ANR, France). D.J.M. was funded by NERC (NE/G014744/1).

Author Contributions R.S. and S.L.C.G. designed and conducted the study; R.S.L. was involved in the conceptual development; S.L.C.G., C.T., M.B., M.V.Z., C.M.M. and S.A.H. all contributed data; K.C. was involved in sample analyses; and K.S. coordinated the PELAGRA deployments. T.R.A. and D.J.M. developed the model and implemented it for field data interpretation; S.L.C.G. analysed the data and wrote the manuscript together with R.S., D.J.M. and T.R.A. All authors discussed and commented on the manuscript.

Author Information Reprints and permissions information is available at www.nature.com/reprints. The authors declare no competing financial interests. Readers are welcome to comment on the online version of the paper. Correspondence and requests for materials should be addressed to T.R.A. (tra@noc.ac.uk, for model R code) or S.L.C.G. (s.giering@abdn.ac.uk, for all other aspects of this work).

METHODS

Cruise details. A multidisciplinary cruise was undertaken at the PAP site (49.0 °N, 16.5 °W) from 8 July to 13 August 2009 aboard RRS *Discovery*.

Particulate flux measurements. Sinking flux of POC was measured at five depths (51, 184, 312, 446 and 589 m) concurrently, using free-drifting, neutrally buoyant traps called PELAGRA (Particle Export measurement using a LAGRAngian trap)[12]. Sample cups for each trap were filled with filtered seawater of 5 p.p.t. excess salinity and sufficient chloroform to give a saturated solution. Traps were deployed with sample cups closed; after a 24-h period to reach and stabilize at the programmed depth, the cups opened and collected sinking material for 48 h, before closing immediately before ascent to the surface. From each trap, two sample cups were combined, screened through a 350-μm mesh to remove swimmers, and split equally into eight aliquots for different analyses. POC-designated splits were filtered at sea through one or more pre-combusted (450 °C, 12 h), 25-mm-diameter glass fibre filters; stored frozen (−20 °C); and later fumed with 100 ml of concentrated sulphurous acid for 48 h, dried (60 °C, 24 h) and pelleted in pre-combusted aluminium foil. Analysis was carried out using a Thermo Finnigan Flash EA1112 elemental analyser with acetanilide as the calibration standard.

DOC input. The contribution of DOC to sustaining interior heterotrophic respiration was calculated, following ref. 15, by assuming that the utilization of primary elements in the twilight zone generally follows the Redfield ratio. We used previous data collected near the PAP site during Atlantic Meridional Transect (AMT) cruises 16 and 17 in May–June 2005 (https://www.bodc.ac.uk/data/published_data_library/catalogue/10.5285/f3b3d4e9-5ede-2824-e044-000b5de50f38/) and October–November 2005 (https://www.bodc.ac.uk/data/published_data_library/catalogue/10.5285/f3b3d4e9-5edf-2824-e044-000b5de50f38/). DOC shows the characteristic surface enhancement (up to 70 μM) with a reduction to 55 μM at 300 m (ref. 29). The profiles show little variability, implying that the supply of DOC is almost constant with season (Extended Data Fig. 2a). Extended Data Fig. 2b shows the regression between apparent oxygen utilization (AOU) and DOC, and the theoretical relationship that would occur if all AOU were due to DOC degradation (C_{org}/O_2 ratio of 117:170). The ratio between the two gradients is 0.377, suggesting that DOC explains 38% of the respiration between 57–300 m. This is consistent with an estimated contribution of DOC respiration to total AOU of 18–47% in the upper 500 m across the South Pacific and Indian oceans[15]. Assuming that sinking POC flux attenuation between 57 and 300 m (49 mg C m^{-2} d^{-1}) made up the remaining 62%, DOC contributed 30 mg C m^{-2} d^{-1} to the carbon flux.

An alternative calculation uses turbulent diffusivity measurements at the PAP site[16], coupled with the aforementioned DOC profiles. The flux of DOC into the twilight zone (F_{DOC}) can be calculated as

$$F_{DOC} = k(\Delta DOC/\Delta z)$$

where k is the diffusivity[16] (10^{-5}–10^{-4} m^2 s^{-1}), Δz is the depth interval (57–300 m) and ΔDOC is the concentration gradient across this depth interval (10 μM). The estimated export of DOC into the twilight zone via turbulent mixing was 0.4–4 mg C m^{-2} d^{-1}. This process does not include DOC fluxes out of the mixed layer from mesoscale processes, and the true DOC export is likely to be closer to the first estimate, of 30 mg C m^{-2} d^{-1}. On the basis of the two estimates of DOC export, we applied a conservative value of 15 mg C m^{-2} d^{-1} for the construction of the twilight zone carbon budget at the PAP site.

Lateral advection. Surface ocean currents derived from satellite altimeter and scatterometer data were downloaded from the NOAA OSCAR website (http://www.oscar.noaa.gov/). The obtained currents encompass both the geostrophic and the wind-driven (Ekman) motion and are available at 1/3°, 5-d resolution. Particles were tracked back in time for 3 months from the initial deployment date of the PELAGRA and ARIES instruments.

Distinction between respiration and carbon demand. The construction of an ecosystem carbon budget is dependent on the definition of input and output terms. If the input is defined as the net supply of organic carbon (the flux entering the twilight zone less that exiting at the base), then the analogous output is the removal of organic carbon via conversion to inorganic carbon during respiration. Respiration differs from the frequently used 'carbon demand'[4–7,30,31] because the latter is quantified as either 'ingestion' or 'ingestion minus egestion' and is therefore an unconstrained quantity. Consider a zooplankton grazer: in the steady state, its carbon demand (that is, ingestion) is balanced by the sum of biomass production (growth and reproduction), excretion, respiration and faecal production[32]. Except for respiration, these processes all produce organic matter that becomes available as food for other heterotrophic organisms such as carnivores or detritivores. In other words, organic carbon is retained and recycled in the system and any one carbon atom may be recycled many times with carbon demand exceeding (being unconstrained by) carbon supply[33,34]. In contrast, each carbon atom within organic matter can only be respired once, ending its journey in the food web, such that, in the steady state, respiration equals carbon supply. A similar phenomenon occurs when (incorrectly, as has often been the case) comparing bacterial carbon demand with primary production, the correct ratio being bacterial respiration to primary production[34,35].

To illustrate the impact that making the distinction between respiration and carbon demand has on the calculation of the twilight-zone carbon budget, we calculated carbon demand from our data following ref. 6 over a similar depth range (150–1,000 m) to allow direct comparability. We then compared our estimates to the observations from the North Pacific[6]. Prokaryotic carbon demand (PCD) was calculated as

$$PCD = PHP \times PGE^{-1}$$

where PHP is prokaryotic heterotrophic production measured using tritiated leucine, and PGE is a prokaryotic growth efficiency of 0.15 (as in ref. 6). Zooplankton carbon demand (ZCD) was estimated as

$$ZCD = ZR \times (1 - NGE)^{-1} \times AE^{-1}$$

where ZR is the allometrically determined respiration rate[36–38], NGE is the net growth efficiency (0.5, as in ref. 6) and AE is the absorption efficiency (0.6, as in ref. 6).

Our modified budget for the North Atlantic is qualitatively similar to the observations from the oligotrophic subtropical (station 'ALOHA') and mesotrophic subarctic (station 'K2') Pacific[6] (Extended Data Fig. 8). In all cases, the sum of the prokaryotic and zooplankton carbon demands exceeds the supply of carbon to the system by a factor of 5–20. This contrasts with the balanced carbon budget we originally calculated at the PAP site. Three key aspects of our original data analyses (use of respiration rather than carbon demand, exclusion of vertical migrators from respiration estimates, and the use of a depth range of 50–1,000 m for the twilight zone) are critical in balancing the twilight zone carbon budget.

Zooplankton collection and preparation. Four vertical, high-resolution profiles of zooplankton biomass and abundance were collected in association with the sediment-trap deployments: one during the day and one at night, at both the beginning and end of the observational period (Table 1). Zooplankton were sampled at 80-m depth intervals from 0–1,000 m using ARIES (the Autosampling and Recording Instrumented Environmental Sampling System) fitted with 200-μm filtering cod-ends. Samples were preserved in 4% saline formaldehyde solution. On shore, the preserved samples were size-fractionated (50–200, 200–350, 350–500, 500–1,000, 1,000–2,000, >2,000 μm) using stacked mesh dishes (Spartel), rinsed with ammonium formate (35.31 g l^{-1}), classified and enumerated. One to 50 individuals (dependent on size) of each group at each depth and size fraction were transferred into pre-weighed tin cups, dried (70 °C, 24 h) and weighed. Biomass (mg dry weight m^{-3}; Extended Data Fig. 3a, b) and abundance (individuals m^{-3}) were calculated for each depth interval.

Zooplankton respiration and excretion. Zooplankton respiration (ZR; μg C individual^{-1} h^{-1}) was estimated from net samples as a function of body mass (DW; mg dry weight individual^{-1}) and temperature (T; °C) using

$$ZR = \exp(a_1 + a_2 \ln(DW) + a_3 T) \times RQ \times 12/22.4$$

where RQ = 0.8 is the respiratory quotient and 12/22.4 is the molar conversion factor[36–38]. For copepods, the parameters a_1, a_2 and a_3 were −0.399, 0.801 and 0.069, respectively[37]. For other zooplankton, the respective parameters were −0.251, 0.789 and 0.049 (ref. 36). Day and night respirations were calculated for 15 and 9 h, respectively, according to the local photoperiod.

Excretion at depth via the active flux was estimated by assuming that DOC excretion by migrating zooplankton is equivalent to 31% of their respiration[18].

Ingestion by vertically migrating zooplankton. Typical vertical migration patterns were observed during both deployments (Extended Data Fig. 3c, d), with large copepods and euphausiids dominating the migrating zooplankton. We assume that at depth these organisms respire material which they have ingested at the surface, and test this assumption using the equation

$$I_{ML} = F_{ind} c_{POC} n_{ML} t$$

where I_{ML} is the total ingested carbon in the mixed layer (mg POC m^{-2} d^{-1}), F_{ind} is the average clearance rate (ml individual^{-1} d^{-1}), c_{POC} is the concentration of POC in the mixed layer[13] (97 mg POC m^{-3}), n_{ML} represents the number of zooplankton in the mixed layer (7,170 and 10,370 individuals m^{-2} during the two deployment periods, respectively) and t is the time that migratory zooplankton spend in the mixed layer each night according to ADCP back-scatter profiles (9 h). Using reported clearance rates of 72–432 ml d^{-1} individual^{-1} for *Calanus*[32,39,40] and 360–2,400 ml d^{-1} individual^{-1} for euphausiids[41,42], total ingestion rates ranged from 18 to 905 mg C m^{-2} d^{-1}.

The daily respiration rates of migratory zooplankton (estimated as for resident zooplankton) were 8 mg C m^{-2} d^{-1}, which is much lower than the calculated ingestion rates. This suggests that migrating zooplankton were able to ingest sufficient organic carbon in the mixed layer to satisfy their respiration, as well as other

physiological processes such as growth, egestion and excretion. It is noteworthy that the strong coupling between daily vertical migration and environmental variables means that migration patterns and associated carbon cycling may change in response to climate change[43].

Prokaryotic leucine incorporation. Incorporation rates of radiolabelled leucine[21] were measured following two protocols: time-course experiments[44] and concentration-series bioassays[45,46]. For the time-course experiments, samples were taken from four depths at four stations in association with the trap deployments (Extended Data Table 1). L-[3,4,5-^{3}H(N)]leucine (specific activity, 115.4 Ci mmol^{-1}; Perkin Elmer) was added to give final concentrations of 20 and 10 nM in triplicate 20- and 40-ml samples from the mixed layer and upper twilight zone (50–150 m) and the lower twilight zone (150–1,000 m), respectively. Respective samples were incubated for 4 and 8 h in sterile Falcon vials in the dark at *in situ* temperatures. The samples were fixed with formaldehyde (2% final concentration).

For the concentration-series bioassays, 2-l water samples were collected from different depths throughout the cruise. L-[4,5-^{3}H]leucine (specific activity, 5.26 TBq mmol^{-1}; Hartmann Analytic) was added in a range of six final leucine concentrations from 0.025 to 0.5 nM. Four samples (1.6 ml each) for each added concentration, that is, 24 samples in total, were incubated in 2-ml capped, screw-top, sterile polypropylene microcentrifuge tubes in the dark at *in situ* temperatures. One of the samples for each concentration was fixed at 0.5, 1, 1.5 or 2 h, respectively, by adding paraformaldehyde (PFA) to 1% final concentration.

All sample particulate material was harvested onto 25-mm-diameter, 0.2-μm polycarbonate filters soaked in unlabelled leucine to reduce background sorption. Filters were washed twice with 4 ml of deionised water (Milli-Q system, Millipore). Radioactivity retained on filters was measured as disintegrations per minute using a liquid scintillation counter (Tri-Carb 3100, Perkin Elmer). Turnover time and estimates of leucine incorporation rate at ambient concentrations from the concentration-series bioassays were calculated following ref. 46. Leucine incorporation rates determined using the two methods agreed well, and there seemed to be little spatial or temporal variability in the twilight zone. All data were therefore pooled for the calculation of prokaryotic respiration.

Prokaryotic respiration. The estimation of prokaryotic respiration (PR) based on measured leucine incorporation rates requires two conversion factors, LeuCF and PGE:

$$\mathrm{PR} = \text{leucine incorporation} \times \mathrm{LeuCF} \times (1 - \mathrm{PGE}) \times \mathrm{PGE}^{-1}$$

LeuCF is the leucine-to-carbon conversion factor, and PGE is the prokaryotic growth efficiency. We reviewed all PGEs and LeuCFs determined for the twilight zone (Extended Data Fig. 4a, b) and estimated prokaryotic respiration (and error margins) using bootstrap analysis with 100,000 simulations (Extended Data Fig. 4c).

The simulations were done as follows. Integrated leucine incorporation rates were determined using the measured leucine incorporation rates at our site. A power-law distribution was fitted to the bootstrap sample ($P < 0.001$, $R^2 = 0.86$, $n = 37$), interpolated (50–1,000 m) and summed to get the integrated incorporation rate. The resulting leucine incorporation rates had a median of 14.5 μmol Leu m^{-2} d^{-1} (interquartile range, 13.2–16.1 μmol Leu m^{-2} d^{-1}). LeuCFs for the simulation were randomly sampled (with replacement) from all reported LeuCFs for the twilight zone[47–50] ($n = 21$). The mean LeuCF used in the simulation was 0.44 kg C mol^{-1} Leu (± 0.27 s.d.). Finally, PGEs were randomly sampled (with replacement) from all reported PGEs for the twilight zone of the North Atlantic[48,51–54] ($n = 26$). PGEs ranged from 0.001 to 0.24 and had a median of 0.08 (interquartile range, 0.04–0.12).

The final estimate of prokaryotic respiration is very sensitive to the interpolation method as well as the two conversion factors (LeuCF and PGE). Our study lacks measurements of leucine incorporation rates from the region between the mixed-layer depth (50 m) and 150 m, which is where most of the POC is remineralized. To arrive at an integrated estimate for leucine incorporation, we chose to interpolate the available leucine incorporation rates using a power-law function because we assume that prokaryotic production in this region is driven by the supply of organic carbon[22], which is best described by a power-law function[9]. The choice of interpolation method introduces additional, large uncertainties into our estimate, potentially leading to a misestimate of integrated leucine incorporation. We recommend that future studies should avoid this uncertainty by increasing sampling effort in this critical region.

Food-web model. The food-web analysis (Extended Data Fig. 6a) is based on the steady-state model of ref. 26. The starting point in ref. 26 is POC input to the twilight zone via sinking detritus. The biological utilization and subsequent respiration of this carbon is then traced along three pathways: colonization, solubilization and production by attached prokaryotes; production of free-living prokaryotes fuelled by DOC generated as a product of solubilization; and consumption by detritivorous zooplankton. We use a new version of this model that maintains these pathways, but with two adjustments.

First, carbon input to the twilight zone now includes both sinking detritus and DOC, the latter representing both vertical mixing and active transport via migratory zooplankton. Second, detritus is divided between sinking and suspended forms (ref. 26 included only the former). It was assumed in ref. 26 that zooplankton losses due to sloppy feeding are in the form of DOC. It may, however, be the case that, particularly for copepods feeding on detritus, much of this loss is as fragmentation (so-called coprorhexy[25]) leading to the generation of small, non-sinking particles.

In the new version of the model, detritus is therefore divided between sinking material (D1), with inputs from surface ocean export and faecal pellet production by detritivores and carnivores, and suspended detritus (D2), which is derived from coprorhexy by detritivores and carnivores and as faecal pellet production by microzooplankton ('prokaryote consumers'). D1 is consumed by both detritivorous zooplankton and attached prokaryotes[26], whereas D2 is acted on only by the prokaryotes.

The model was reparameterized as follows (see Extended Data Table 2 for the list of parameters). Parameter ψ_B, the partitioning of detritus consumption by attached prokaryotes and detritivores, is poorly known and was estimated as 0.75 (75% prokaryotes, 25% zooplankton) in ref. 26, on the basis of the data of ref. 6. Using the data from the PAP site, we were better able to constrain this parameter and use a value of $\psi_B = 0.5$ (see sensitivity analysis below). Of the POC (D1 and D2) acted on by attached prokaryotes, 50% is solubilized by the action of hydrolytic enzymes and released as DOC[26] (parameter α). PGEs for free-living and attached prokaryotes (ω_{fl} and ω_{att}) were set to 0.08 and 0.24, respectively. The former value is based on the literature review presented above and the latter comes from ref. 26. Release of DOC as excretion by prokaryote consumers, detritivores and carnivores was set at 5% of processed prey items[26] (Φ_V, Φ_H, $\Phi_Z = 0.05$). The corresponding fraction allocated to D2 via sloppy feeding was set as $\lambda_H = 0.30$ for detritivores (based on Fig. 2 of ref. 25), thereby assuming that a large fraction of processed food is released as non-pellet POC, with a value of $\lambda_Z = 0.15$ for carnivores. Sloppy-feeding losses by prokaryote consumers were assumed to be zero ($\lambda_V = 0$) because they ingest their prey whole. Absorption efficiencies (also commonly known as assimilation efficiencies) were assigned values of $\beta_H = 0.60$, $\beta_Z = 0.66$ and $\beta_V = 0.72$ (refs 26, 55). The fraction of prey items that is absorbed across the gut is $\beta(1 - \Phi)(1 - \lambda)$, this material being used with net production efficiencies for detritivores, carnivores and bacterivores (κ_H, κ_Z and κ_V) of 0.39, 0.39 and 0.44, respectively[26]. Finally, parameter ζ, the fraction of attached prokaryotes consumed by detritivores (rather than prokaryote consumers) was assigned a value of 0.24 (ref. 26).

In ref. 26, steady-state equations were derived and the model was constructed in a Microsoft Excel spreadsheet. The modifications to the model here (direct DOC input, detritus divided into D1 and D2) make a steady-state solution difficult and so we instead constructed two versions of the model in R, the first a Monte Carlo version and the second a dynamic version that is run until a steady state is reached (we show results for the latter, which is deterministic).

Sensitivity analysis. An analysis of the steady-state solution of the model is presented in Extended Data Fig. 6b–d. Inputs of carbon to the twilight zone, namely POC (74 mg C m^{-2} d^{-1}) and DOC (18 mg C m^{-2} d^{-1}) are balanced by community respiration, which is the sum of attached and free-living prokaryotes (23.9 and 48.6 mg C m^{-2} d^{-1}, respectively) and detritivores, carnivores and prokaryote consumers (11.0, 3.3 and 5.1 mg C m^{-2} d^{-1}, respectively). The main detritus source is export of sinking particles from the surface ocean, supplemented by *in situ* faecal pellet production by detritivores and carnivores. Although detritivores and attached prokaryotes each utilize 50% of D1 (parameter ψ_B), it is the attached prokaryotes that undertake the majority of POC utilization overall (57% versus 43%) because they are the sole consumers of D2. Finally, the largest DOC source in the model is solubilization of detritus by attached prokaryotes (31.5 mg C m^{-2} d^{-1}), which is greater than the input from the surface ocean (18 mg C m^{-2} d^{-1}). Utilization of DOC is exclusively by free-living prokaryotes. Overall, the results highlight the importance of both zooplankton and prokaryotes in the carbon cycle of the twilight zone, the former primarily as recyclers and the latter as a carbon sink (Fig. 2).

The robustness of the model results and conclusions with respect to chosen parameter values were investigated by undertaking sensitivity analyses. Parameter ψ_B (the fraction of D1 acted on by attached prokaryotes, the remainder by detritivorous zooplankton) was varied between 0.1 and 0.9 (standard value, 0.5), λ_H (the loss to D2 by sloppy feeding by detritivores) was varied between 0.1 and 0.5 (standard value, 0.3), and ω_{fl} (PGE for free-living prokaryotes) was assigned values of 0.04, 0.08 (standard) and 0.12. The resulting predictions for respiration by zooplankton and prokaryotes are shown in Extended Data Fig. 7; the point of interest is the parameter ranges, which are consistent with measured estimates of respiration, that is, ZR = 14 mg C m^{-2} d^{-1} and PR = 71 mg C m^{-2} d^{-1}. ZR predicted by the model, excluding respiration by microzooplankton (prokaryote consumers), is 14.3 mg C m^{-2} d^{-1} using parameter settings $\psi_B = 0.5$ and $\lambda_H = 0.3$. Extended Data Fig. 7c, d (PGE = 0.08) shows that the best solution for ZR (14.3 mg C m^{-2} d^{-1}) is achieved with $\psi_B = 0.5$, that is, with detritivores and attached bacteria processing half each of D1, and with detritivores releasing 30% of their half

as suspended POC (D2). The required zooplankton contribution to processing sinking POC (D1) decreases if less processed D1 is allocated to D2 (in which case more is respired), but not to any great extent. For example, decreasing suspended losses (parameter λ_H) from 30% to 10% means that the required ZR (to match the data) is achieved with $\psi_B = 0.63$, that is, detritivores processing 37% of D1. We conclude that the model predictions are robust with respect to a mid-range value of ψ_B, for example 0.5.

PGE is notoriously low in the twilight zone of the ocean[48,51–54]. Visual inspection of Extended Data Fig. 7 shows that predicted ZR and PR are remarkably insensitive to ω_{fl}. For example, decreasing ω_{fl} to 0.04 (half the standard value) meant that predicted ZR (for $\psi_B = 0.5$ and $\lambda_H = 0.3$) decreased from 14.3 to 14.0 mg C m^{-2} d^{-1} and that PR increased from 72.5 to 73.7 mg C m^{-2} d^{-1}. The relative insensitivity is easy to explain in that prokaryotes are the main sink for carbon and so decreasing PGE just strengthens this. Likewise, increasing ω_{fl} to 0.12 has only a minor impact on model results (Extended Data Fig. 7e,f). Predicted ZR for $\psi_B = 0.5$ and $\lambda_H = 0.3$ increases to 14.6 mg C m^{-2} d^{-1} as carbon transfer to higher trophic levels is increased, whereas PR decreases to 71.3 mg C m^{-2} d^{-1}.

Overall, the results are robust to changes in PGE, as well as to changes in detritivore sloppy-feeding losses (λ_H). Model solutions indicate that a mid-range value of parameter ψ_B, in the region of 0.5, is required to match the observational data, and thus confirms the overall conclusion of the synergistic role of zooplankton and prokaryotes in carbon cycling in the twilight zone of the ocean.

29. Hansell, D. A., Carlson, C. A. & Schlitzer, R. Net removal of major marine dissolved organic carbon fractions in the subsurface ocean. *Glob. Biogeochem. Cycles* **26,** GB1016 (2012).
30. Sasaki, H., Hattori, H. & Nishizawa, S. Downward flux of particulate organic matter and vertical distribution of calanoid copepods in the Oyashio water in summer. *Deep-Sea Res.* **35,** 505–515 (1988).
31. Yamaguchi, A. *et al.* Community and trophic structures of pelagic copepods down to greater depths in the western subarctic Pacific (WEST-COSMIC). *Deep-Sea Res. I* **49,** 1007–1025 (2002).
32. Mayor, D. J., Anderson, T. R., Pond, D. W. & Irigoien, X. Egg production and associated losses of carbon, nitrogen and fatty acids from maternal biomass in *Calanus finmarchicus* before the spring bloom. *J. Mar. Syst.* **78,** 505–510 (2009).
33. Strayer, D. On the limits to secondary production. *Limnol. Oceanogr.* **33,** 1217–1220 (1988).
34. Legendre, L. & Rivkin, R. Planktonic food web: microbial hub approach. *Mar. Ecol. Prog. Ser.* **365,** 289–309 (2008).
35. Anderson, T. R. & Ducklow, H. W. Microbial loop carbon cycling in ocean environments studied using a simply steady-state model. *Aquat. Microb. Ecol.* **26,** 37–49 (2001).
36. Ikeda, T. Metabolic rates of epipelagic marine zooplankton as a function of body mass and temperature. *Mar. Biol.* **85,** 1–11 (1985).
37. Ikeda, T., Kanno, Y., Ozaki, K. & Shinada, A. Metabolic rates of epipelagic marine copepods as a function of body mass and temperature. *Mar. Biol.* **139,** 587–596 (2001).
38. Al-Mutairi, H. & Landry, M. R. Active export of carbon and nitrogen at Station ALOHA by diel migrant zooplankton. *Deep-Sea Res. II* **48,** 2083–2103 (2001).
39. Fileman, E., Smith, T. & Harris, R. Grazing by *Calanus helgolandicus* and *Para-Pseudocalanus* spp. on phytoplankton and protozooplankton during the spring bloom in the Celtic Sea. *J. Exp. Mar. Biol. Ecol.* **348,** 70–84 (2007).
40. Mayor, D. J., Anderson, T. R., Irigoien, X. & Harris, R. Feeding and reproduction of *Calanus finmarchicus* during non-bloom conditions in the Irminger Sea. *J. Plankton Res.* **28,** 1167–1179 (2006).
41. Ohman, M. Omnivory by *Euphausia pacifica*: the role of copepod prey. *Mar. Ecol. Prog. Ser.* **19,** 125–131 (1984).
42. McClatchie, S. Time-series feeding rates of the euphausiid *Thysanoessa raschii* in a temporally patchy food environment. *Limnol. Oceanogr.* **31,** 469–477 (1986).
43. Bianchi, D., Galbraith, E. D., Carozza, D. A., Mislan, K. A. S. & Stock, C. A. Intensification of open-ocean oxygen depletion by vertically migrating animals. *Nature Geosci.* **6,** 545–548 (2013).
44. Tamburini, C., Garcin, J., Ragot, M. & Bianchi, A. Biopolymer hydrolysis and bacterial production under ambient hydrostatic pressure through a 2000 m water column in the NW Mediterranean. *Deep-Sea Res. II* **49,** 2109–2123 (2002).
45. Wright, R. T. & Hobbie, J. E. Use of glucose and acetate by bacteria and algae in aquatic ecosystems. *Ecology* **47,** 447–464 (1966).
46. Zubkov, M. V., Tarran, G. A., Mary, I. & Fuchs, B. M. Differential microbial uptake of dissolved amino acids and amino sugars in surface waters of the Atlantic Ocean. *J. Plankton Res.* **30,** 211–220 (2008).
47. Alonso-Sáez, L. *et al.* Large-scale variability in surface bacterial carbon demand and growth efficiency in the subtropical northeast Atlantic Ocean. *Limnol. Oceanogr.* **52,** 533–546 (2007).
48. Baltar, F., Arístegui, J., Gasol, J. M., Sintes, E. & Herndl, G. J. Evidence of prokaryotic metabolism on suspended particulate organic matter in the dark waters of the subtropical North Atlantic. *Limnol. Oceanogr.* **54,** 182–193 (2009).
49. Gasol, J. M. *et al.* Mesopelagic prokaryotic bulk and single-cell heterotrophic activity and community composition in the NW Africa–Canary Islands coastal-transition zone. *Prog. Oceanogr.* **83,** 189–196 (2009).
50. del Giorgio, P. *et al.* Coherent patterns in bacterial growth, growth efficiency, and leucine metabolism along a northeastern Pacific inshore-offshore transect. *Limnol. Oceanogr.* **56,** 1–16 (2011).
51. Carlson, C. A. *et al.* Interactions among dissolved organic carbon, microbial processes, and community structure in the mesopelagic zone of the northwestern Sargasso Sea. *Limnol. Oceanogr.* **49,** 1073–1083 (2004).
52. Arístegui, J. Duarte, C. M., Gasol, J. M. & Alonso-Sáez, L. Active mesopelagic prokaryotes support high respiration in the subtropical northeast Atlantic Ocean. *Geophys. Res. Lett.* **32,** L03608 (2005).
53. Reinthaler, T., van Aken, H. M. & Veth, C. Prokaryotic respiration and production in the meso- and bathypelagic realm of the eastern and western North Atlantic basin. *Limnol. Oceanogr.* **51,** 1262–1273 (2006).
54. Baltar, F., Arístegui, J., Gasol, J. M. & Herndl, G. J. Prokaryotic carbon utilization in the dark ocean: growth efficiency, leucine-to-carbon conversion factors, and their relation. *Aquat. Microb. Ecol.* **60,** 227–232 (2010).
55. Mayor, D. J. *et al.* Absorption efficiencies and basal turnover of C, N and fatty acids in a marine Calanoid copepod. *Funct. Ecol.* **25,** 509–518 (2011).

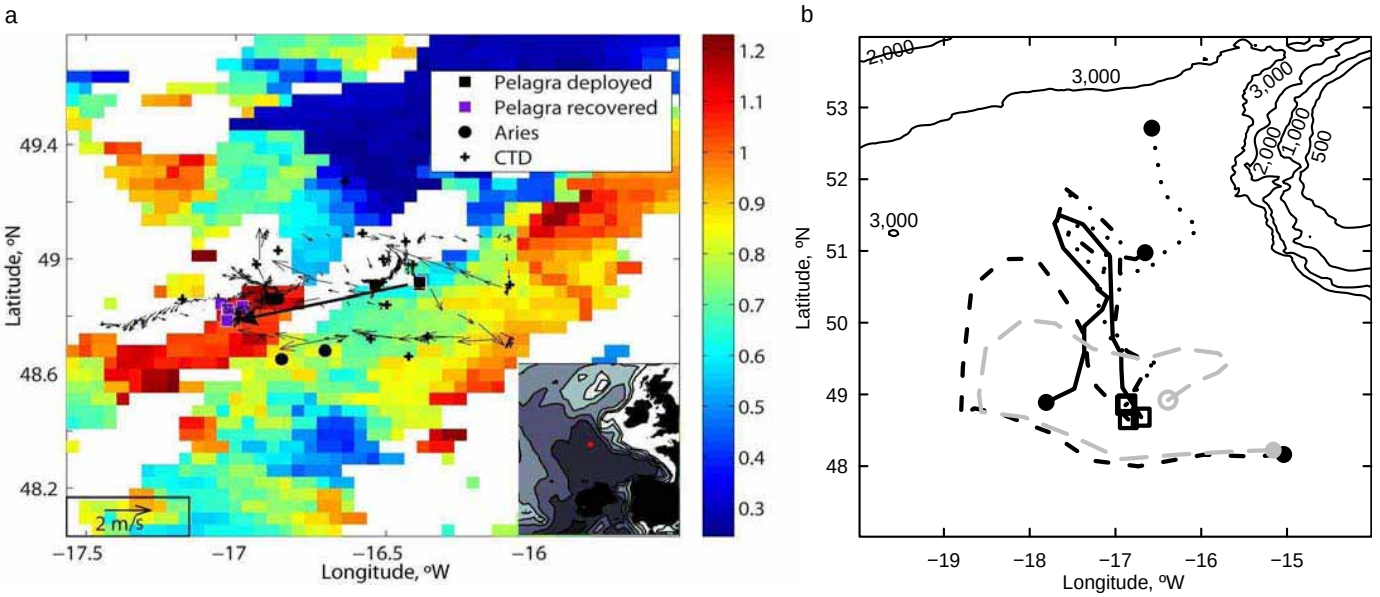

Extended Data Figure 1 | Study site and deployments. **a**, Current vectors from a vessel-mounted acoustic Doppler current profiler (thin black arrows) overlaid on surface chlorophyll (mg m^{-3}; averaged from 28 July to 8 August 2009). The five sediment traps (PELAGRA; squares) followed the edge of an eddy (thick black arrow). Collection sites for zooplankton (ARIES system, circles) and prokaryotes (CTD, crosses) are marked. **b**, Lateral advection to the PAP site. Surface particle back-trajectories of the water masses sampled using PELAGRA (grey) and ARIES (black), calculated from satellite-derived near-surface velocities over 3 months. Particles started at the solid circles.

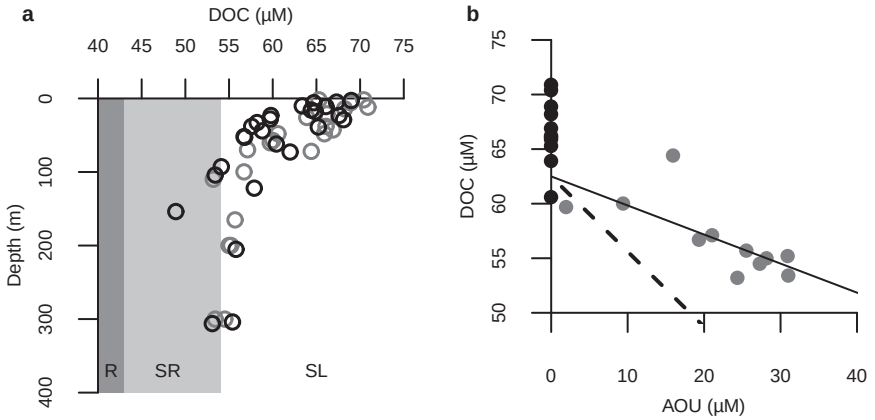

Extended Data Figure 2 | DOC supply to the twilight zone. a, Depth profiles of DOC at the PAP site at four stations during June (grey) and October (black) 2005. Shaded areas represent background concentrations of refractory (R), semi-refractory (SR) and semi-labile (SL) pools based on ref. 29. **b**, The relationship between AOU and DOC at the four stations. Black and grey circles respectively represent samples collected above and below the mixed layer (here 57 m). DOC recorded below 57 m correlates to AOU (grey line: DOC = −0.26AOU + 62.5; $P = 0.01$, $R^2 = 0.53$, $n = 9$). The dotted line represents the theoretical relationship following the Redfield ratio (DOC = −(117/170)AOU + 62.5), which would pertain if all AOU were caused by the respiration of DOC.

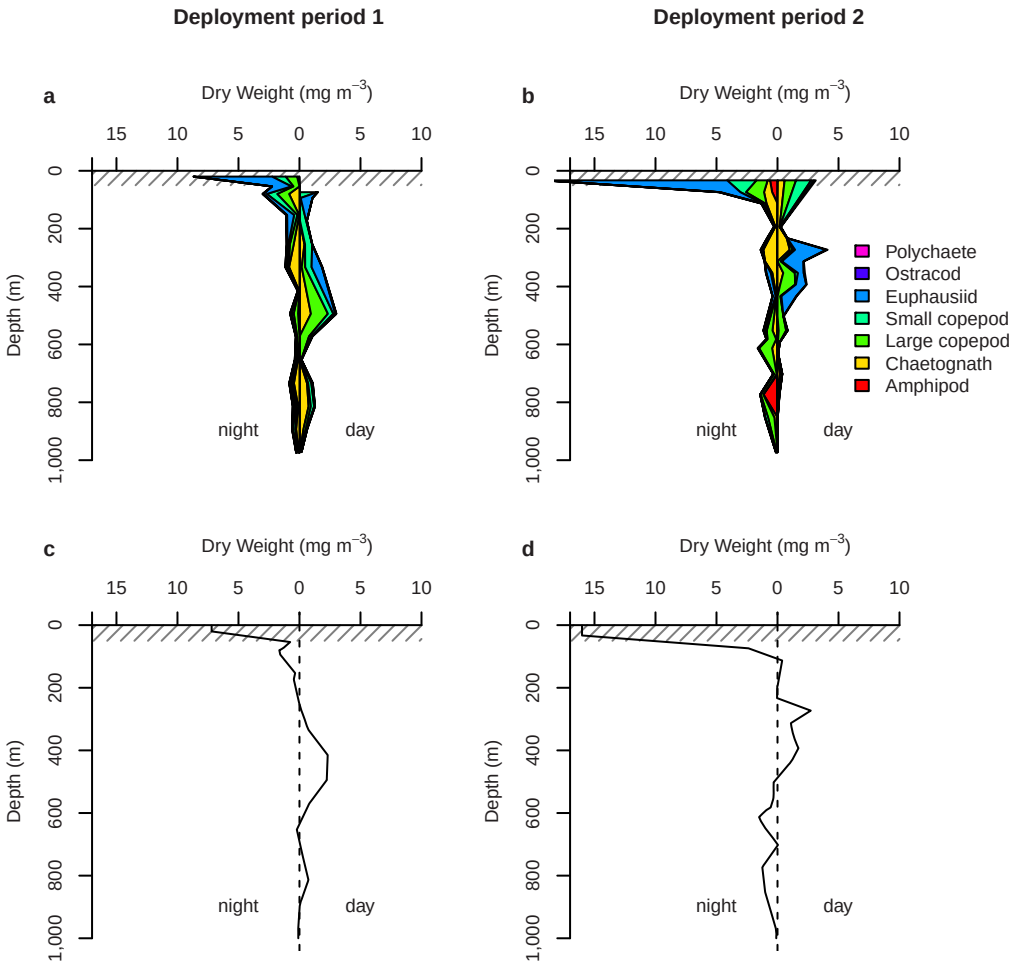

Extended Data Figure 3 | Zooplankton depth distribution. **a**, **b**, Zooplankton biomass (>200 µm) during deployment periods 1 and 2 at the PAP site. Taxonomic groups are colour-coded as shown. **c**, **d**, Biomass of migratory zooplankton during deployment periods 1 and 2. Biomasses of community and migratory zooplankton are represented for daytime (right) and night time (left). The shaded area represents the mixed layer.

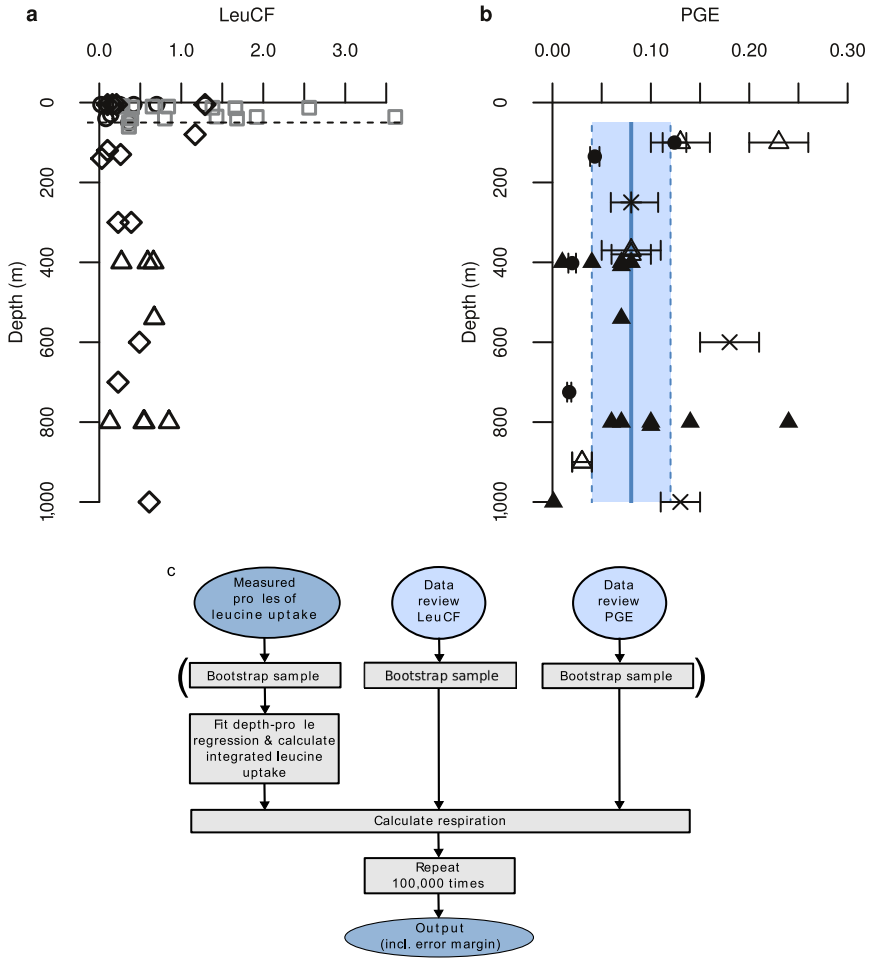

Extended Data Figure 4 | Steps for calculating prokaryotic respiration. **a**, Depth profiles of the leucine-to-carbon conversion factor (LeuCF) measured in the eastern North Atlantic (circles[47], triangles[48] and diamonds[49]) and the North Pacific (grey squares[50]). The average LeuCF below 50 m was 0.44 kg C mol^{-1} Leu (±0.27 s.d., $n = 21$). **b**, Depth profiles of prokaryotic growth efficiency (PGE) measured for the twilight zone across the North Atlantic (open triangles[48], asterisk[51], crosses[52], filled triangles[53] and filled circles[54]). The solid blue line shows the median PGE (0.08, $n = 26$), and the blue shaded area shows the interquartile range (0.04–0.12). Error bars, s.e.m. as reported in original studies. **c**, Flow diagram of calculation of prokaryotic respiration using bootstrapping. The output gives 100,000 estimates of prokaryotic respiration, which are used to compute the uncertainty in the final estimate.

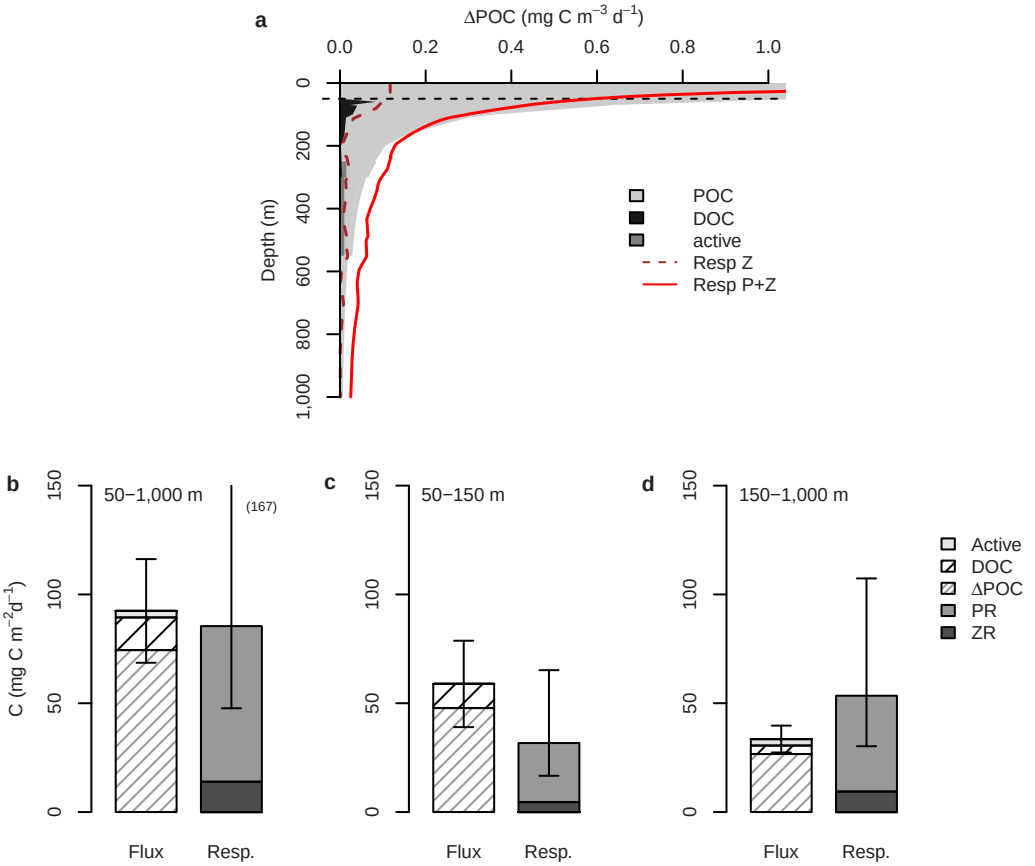

Extended Data Figure 5 | Twilight-zone carbon budget with different depth horizons. **a**, Organic matter supply via dissolved matter (black area), active transport (mid grey area) and total supply including particles (light grey area), compared with zooplankton respiration (dashed red line) and community respiration (prokaryotes plus zooplankton; solid red line). **b**–**d**, Comparison of net supply of organic carbon (sum of active flux, DOC and ΔPOC) with respiration by prokaryotes (PR) and non-migratory zooplankton (ZR) in the entire twilight zone (50–1,000 m; **b**), the upper twilight zone (50–150 m; **c**) and the lower twilight zone (150–1,000 m; **d**). Error bars represent upper and lower estimates (see text).

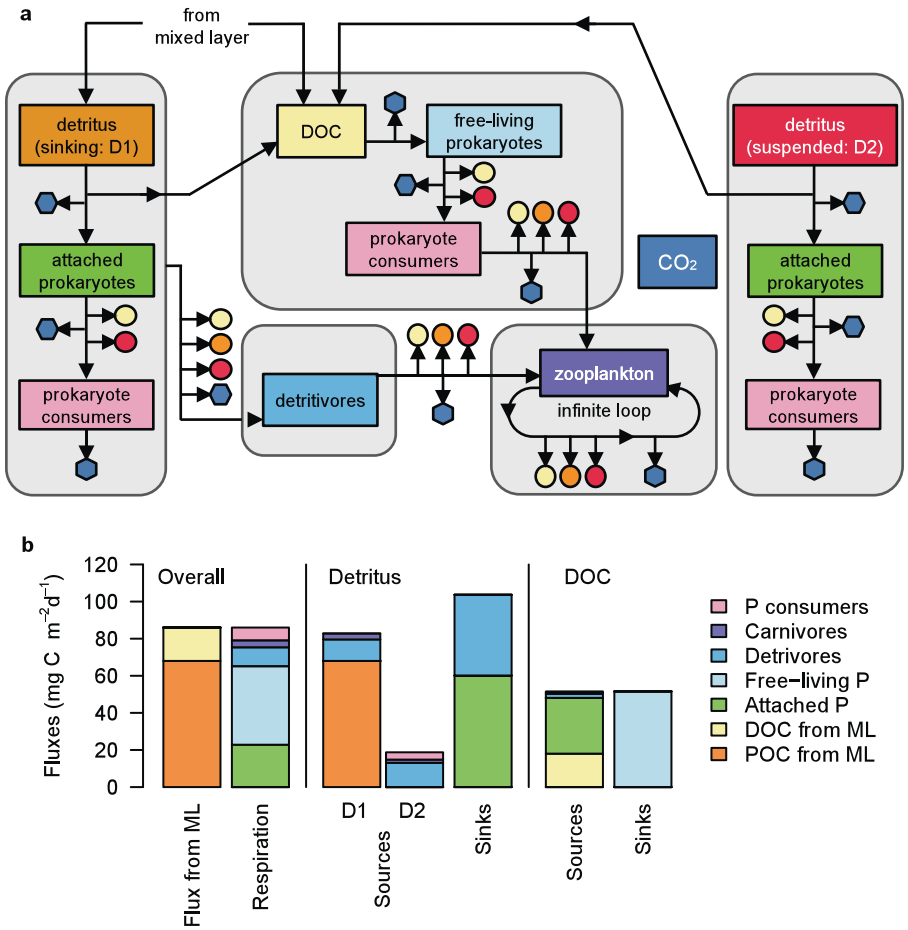

Extended Data Figure 6 | Twilight-zone carbon model. **a**, Flow diagram. Recycling pathways by attached prokaryotes, detritivores and the microbial loop (DOC and free-living prokaryotes). Fluxes to small coloured circles or hexagons enter sinking detritus (D1; orange circles), suspended detritus (D2; red circles), DOC (yellow circles) or CO_2 (blue hexagons). **b**, Modelled sources and sinks of carbon. Net inputs of POC and DOC from the mixed layer (ML) versus respiration by the twilight-zone food web ('Overall'; left); sources (D1 and D2 represent sinking and suspended POC, respectively) and sinks of detritus (middle); and sources and sinks of DOC (right). P, prokaryotes.

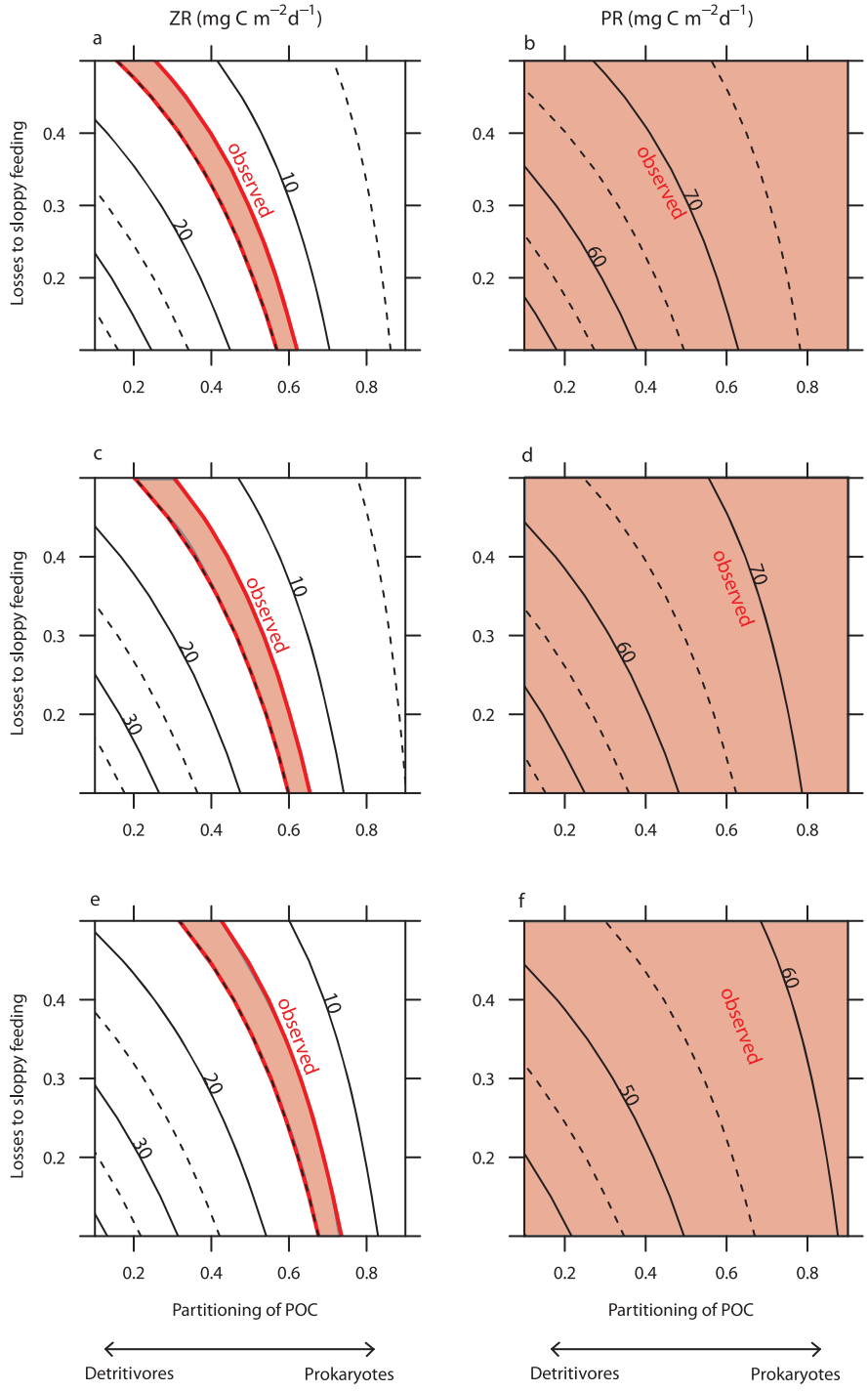

Extended Data Figure 7 | Sensitivity analysis for predicted respiration rates. Predicted zooplankton respiration (ZR; mg C m^{-2} d^{-1}; excluding microzooplankton) and prokaryotic respiration (PR; mg C m^{-2} d^{-1}) for varying parameters. The fraction of sinking POC consumed by attached prokaryotes (ψ_B; remainder consumed by detritivorous zooplankton) was varied between 0.1 and 0.9 (standard model value, 0.5). The fraction of grazed POC that is lost to suspended POC owing to sloppy feeding by detritivores (λ_H) was varied between 0.1 and 0.5 (standard value, 0.3). PGE (ω_{fl}) was assigned values of 0.04 (**a**, **b**), 0.08 (**c**, **d**) and 0.12 (**e**, **f**). Red areas show the estimated range based on field data.

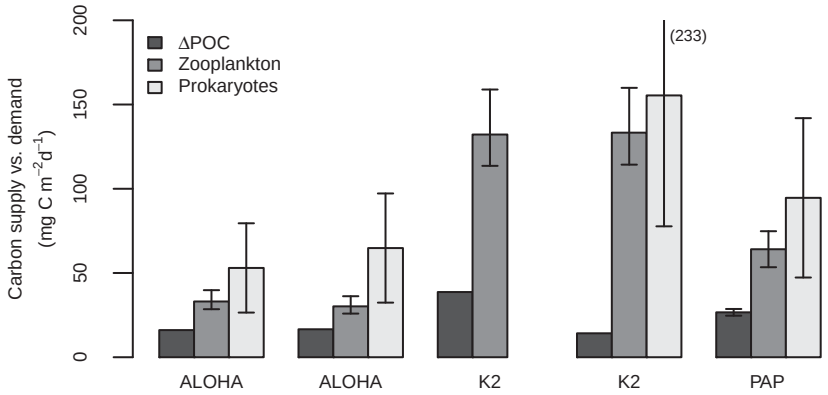

Extended Data Figure 8 | Twilight-zone carbon budgets based on 'carbon demand'. Budgets were compiled by comparing loss of POC (ΔPOC; black) with carbon demand (ingestion) by zooplankton (dark grey) and prokaryotes (light grey) in the North Atlantic (PAP; this study) and twice at each of two stations in the Pacific (ALOHA and K2; ref. 6). The imbalance of these budgets contrasts with our final budget (Fig. 1d) based on respiration. Error bars show analytical errors for POC flux and upper and lower estimates for carbon demands based on a range of conversion factors (see methods reported in ref. 6 for details).

Extended Data Table 1 | Deployment details

Type	Station	Date	Time of day	Latitude (N)		Longitude (W)		Max. depth
			(hh:mm)	deployed	recovered	deployed	recovered	(m)
PELAGRA	P7	03-06/08/09	13:40 - 19:21	48.54.8	48.50.6	16.23.4	17.03.0	589
PELAGRA	P6	03-06/08/09	13:15 - 19:21	48.54.8	48.49.6	16.23.2	17.01.7	446
PELAGRA	P5	03-06/08/09	12:50 - 19:24	48.54.9	48.48.7	16.23.2	17.01.5	312
PELAGRA	P4	03-06/08/09	12:25 - 19:21	48.55.1	48.50.1	16.23.3	16.58.7	184
PELAGRA	P2	03-06/08/09	12:00 - 19:21	48.55.2	48.47.1	16.23.3	17.01.8	51
ARIES	2	08/08/2009	16:01 - 17:48	48.51.3	48.48.6	16.53.0	16.58.6	972
ARIES	2	07/08/2009	21:49 - 23:29	48.51.8	48.48.9	16.51.7	16.57.1	973
ARIES	1	01/08/2009	20:42 - 22:09	48.39.2	48.37.5	16.50.9	16.54.6	974
ARIES	1	01/08/2009	16:09 - 18:00	48.40.9	48.40.3	16.42.2	16.48.9	972
CTD	16514	19/07/2009	17:20 – 18:30	49.01.0	49.02.0	16.30.9	16.51.6	1000
CTD	16606	01/08/2009	10:08 – 13:32	48.41.8	48.40.7	16.33.4	16.34.3	3000
CTD	16616	02/08/2009	22:28 – 00:52	49.03.3	49.02.2	16.26.0	16.26.0	2000
CTD	16640	06/08/2009	15:48 – 18:14	48.55.8	48.33.0	16.30.1	16.32.7	2000

Deployments of neutrally buoyant sediment traps (PELAGRA) and the plankton sampler (ARIES) at the PAP site in August 2009. Sampling of sediment traps commenced 24 h after deployment time and lasted for 48 h. Presented times relate to deployment and recovery of the traps. Depths for PELAGRA deployments are mean depths.

Extended Data Table 2 | Model parameters and default values

Parameter	Description	Value
ψ_B	partitioning of D1 to attached prokaryotes	0.5
α	solubilization losses: attached prokaryotes	0.5
$\acute{\omega}_{att}$	PGE: attached prokaryotes	0.24
$\acute{\omega}_{fl}$	PGE: free-living prokaryotes	0.08
ϕ_V	release of DOC as excretion by prokaryote consumers	0.05
ϕ_H	release of DOC as excretion by detritivores	0.05
ϕ_Z	release of DOC as excretion by carnivores	0.05
λ_V	grazing losses to D2 via sloppy feeding: prokaryote consumers	0
λ_H	grazing losses to D2 via sloppy feeding: detritivores	0.30
λ_Z	grazing losses to D2 via sloppy feeding: carnivores	0.15
β_V	absorption efficiency: prokaryote consumers	0.72
β_H	absorption efficiency: detritivores	0.60
β_Z	absorption efficiency: carnivores	0.66
κ_V	NGE: prokaryote consumers	0.44
κ_H	NGE: detritivores	0.39
κ_Z	NGE: higher zooplankton	0.39
ζ	Particle microbial losses to detritivores	0.24

All parameters are dimensionless.